Journal of *Marine Science and Engineering*

MDPI

Article

Docking Collision Response of an Underwater Mooring Suspension Docking System

Hua Tan [1,2,*], Zhen Lv [1], Rong Zheng [1] and Guangzhi Zhang [1]

[1] State Key Laboratory of Robotics and Intelligent Systems, Shenyang Institute of Automation, Chinese Academy of Sciences, Shenyang 110169, China; lvzhen@sia.cn (Z.L.); zhengr@sia.cn (R.Z.); zhangguangzhi@sia.cn (G.Z.)
[2] University of Chinese Academy of Sciences, Beijing 100049, China
* Correspondence: tanhua@sia.cn

Abstract

Suspension docking systems offer significant application potential in autonomous underwater docking operations because of their deployment and recovery convenience. This study investigated the interaction between an axisymmetric, underactuated autonomous underwater vehicle (AUV) and a suspended guiding hood docking device (DOCK). The effects of collision velocity, collision location, collision angle, mass, and moment of inertia on the post-collision kinematic states of both bodies are analyzed. Previous studies have typically determined AUV parameters using empirical formulas, whereas few have clearly described the calibration procedure for the hydrodynamic drag coefficients of a suspended guiding hood DOCK. In this study, the hydrodynamic coefficients of both the AUV and the DOCK were determined using STAR-CCM+ and embedded into the ADAMS built-in functions to construct a physically more realistic simulation model. Subsequently, water tank experiments were conducted for suspension docking collisions. The validity of the simulation model was verified by comparing the kinematic states of the DOCK and AUV observed from the simulations and experiments. Based on the established model, the docking dynamics under various operating conditions were simulated. The simulation results indicate that the AUV mass should not exceed twice the mass of the DOCK, and the moment of inertia of the DOCK should be maximized. The risk of suspension docking failure increases significantly when the mooring line length exceeds 40 m, and the negative buoyancy of the DOCK should be at least 300 N. These findings provide critical guidance for improving the success rate of suspension docking operations.

Keywords: autonomous underwater vehicle; underwater docking; mooring suspension; suspension docking; collision response

Check for updates

Academic Editor: Weicheng Cui

Received: 19 May 2026
Revised: 26 June 2026
Accepted: 1 July 2026
Published: 4 July 2026

Copyright: © 2026 by the authors. Licensee MDPI, Basel, Switzerland. This article is an open access article distributed under the terms and conditions of the Creative Commons Attribution (CC BY) license.

1. Introduction

Currently, the primary approach to addressing the endurance limitations of autonomous underwater vehicles (AUVs) involves utilizing fixed underwater docking stations for energy replenishment or data exchange [1]. However, because of the substantial base structures associated with such stations, repositioning or adjusting their attitude after seabed deployment is challenging [2], thereby constraining the operational radius of an AUV. To improve the operational flexibility of AUV recovery and the feasibility of sustained observation, numerous researchers have proposed schemes employing unmanned surface vehicles to suspend docking apparatuses [3]. Achieving suspension docking in

this configuration would ensure adequate energy supply for AUVs, enabling them to follow unmanned surface vehicles and execute detection tasks across broader maritime domains. Based on the docking mechanism, suspension docking is generally divided into capture-type and enclosure-type configurations. Although the enclosure type minimizes the need for AUV structural modifications and imposes reduced requirements for navigation accuracy, the overall structure of the guiding hood docking device (DOCK) is relatively complex. Furthermore, existing literature predominantly focuses on developing guidance and motion control strategies for underactuated AUVs to achieve precise homing, whereas in-depth investigations of the collision-coupling dynamics between underactuated AUVs and movable suspended docking stations during terminal docking remain limited [4–6]. Consequently, this paper focuses on optimizing the structure of the enclosure-type docking system to improve docking success rates.

To optimize the system structure, Wu et al. used FLUENT [7] to analyze the effects of flow-field variations induced by guiding hoods of different geometries under various operating conditions. They observed that closed guiding hoods generated greater resistance for the AUV, and they qualitatively proposed an optimal hood geometry for docking. Similarly, Yang et al. [8] employed FLUENT to quantitatively analyze the influence of guiding hood taper angles on an AUV and found that the applicable taper range for docking was 35–55°. Furthermore, they simulated the effect of docking pipe diameter on AUV resistance and found that docking conditions with yaw angles exceeding 30° are more prone to failure. However, given that collisions between the AUV and DOCK are inevitable during the docking process, and considering that the flow-field analyses neglected contact forces, it is crucial to analyze underwater docking collision responses and optimize the structure based on these results. Lin et al. [9] created a suspension collision simulation environment using ADAMS. Using the number of collisions as an evaluation parameter, they analyzed the effects of the mass ratio, eccentricity, and mooring line length on the docking process. Their analyses revealed that a smaller DOCK mass, larger eccentricity, and longer mooring lines contribute to an increased number of collisions, which is detrimental to successful docking. Guo Jingqian et al. [10] investigated the impact of collisions on the docking of a single-point mooring suspension docking system using Star-CCM+. Combining these findings with sea trial results, they explicitly stated that the pitch angle of the DOCK should be limited to 10°. Furthermore, they ranked the critical parameters that influence AUV docking in descending order of importance: DOCK geometry, moment of inertia, mass, and mooring line stiffness.

Although Star CCM+ considers the influence of flow-field variations on docking, its computational cycle is considerably longer, and its hardware requirements are higher than those of ADAMS for simulating identical conditions. Therefore, when utilizing the latter for simulation, many researchers [11,12] applied added mass as a mass force acting on the AUV to simulate the inertial forces exerted by the water flow. Given that research specific to suspension docking systems remains limited, the DOCKs reported in the literature [11–16] were fixed relative to the seabed; consequently, considerations for added mass coefficients were unnecessary when defining loads for the DOCKs. Moreover, although the DOCKs in [9,17,18] were not fixed relative to the ground, these studies did not explicitly detail the methodology for setting the hydrodynamic drag parameters of the DOCKs.

This paper focuses on a revolution-body AUV with a diameter of 534 mm and its corresponding DOCK, which are used in practice [19] (Figure 1). To simplify the computations, a quiescent water environment was assumed throughout the docking simulation. In addition, the suspension point of the mooring line was assumed to remain fixed relative to the ground. The suspension docking process was simulated using ADAMS, with the setting of hydrodynamic drag coefficients for the AUV and DOCK serving as the entry point. The

collision responses under varying conditions of collision velocity, eccentricity, offset angle, negative buoyancy, moment of inertia, and mass were analyzed. The applicability of the parameters within the simulation environment was validated through water tank experiments. This study lays a crucial foundation for establishing stable and efficient suspension docking strategies to mitigate attitude instability of DOCKs following collision impacts.

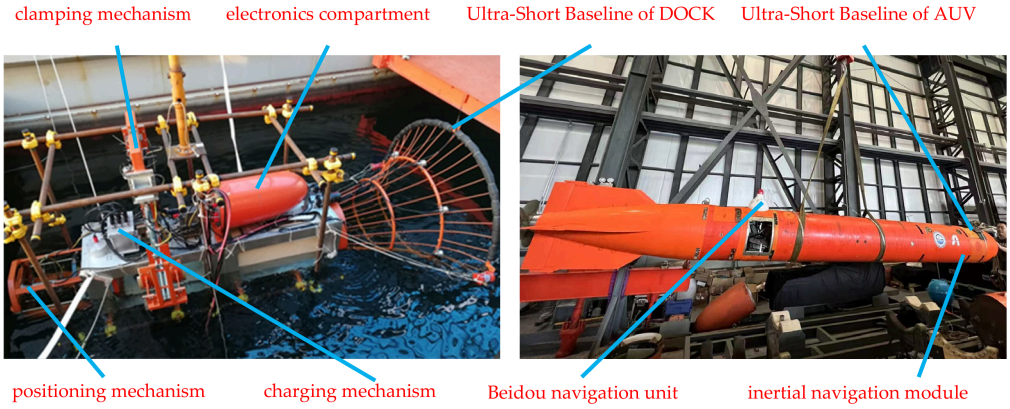


Figure 1. Prototype of the docking system.

2. Establishment of the Mathematical Model

The DOCK is suspended from a fixed point via a mooring line, maintaining a static-equilibrium state within the aquatic environment (Figure 2). The AUV maintains an initial separation distance of 10 m from the DOCK. Upon initiation of the docking maneuver, the AUV approaches the DOCK at a constant velocity, subject to gravitational forces, buoyancy, main propeller thrust, hydrodynamic drag, and collision forces. In contrast, although the DOCK lacks the main propeller thrust, it is subjected to an additional mooring-line tension force. The self-weight of the mooring line is neglected, given that it has a length (L_0) of 10 m and a diameter of 1 cm. By integrating the experimental conditions into the simulation environment, the following fundamental assumptions are posited.

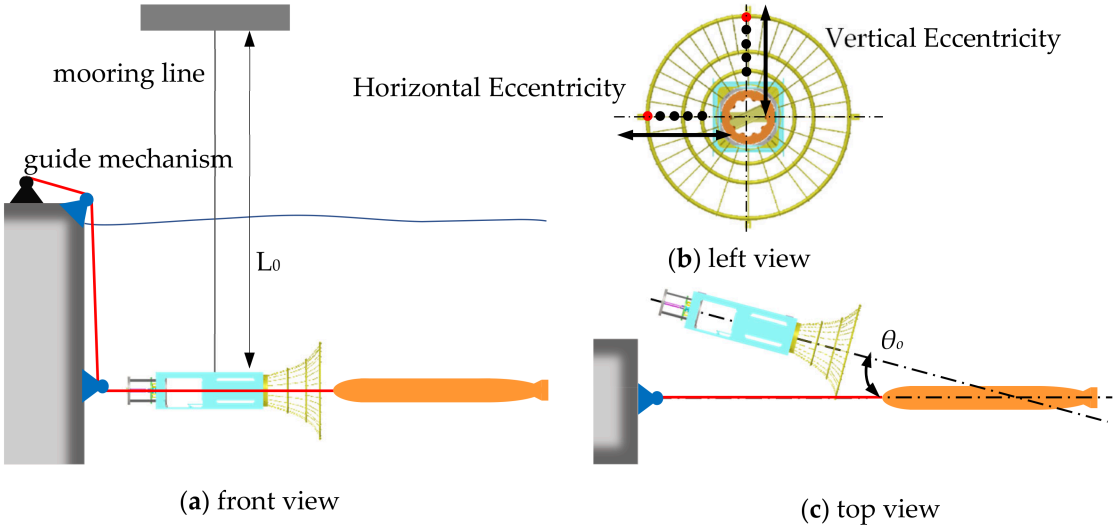


Figure 2. Suspended docking test schematic diagram.

1. Both the AUV and DOCK are homogeneous bodies.
2. The gravitational and buoyant forces acting on the AUV are mutually canceling.
3. The self-weight and axial hydrodynamic drag of the mooring line are neglected; only elastic forces and radial hydrodynamic drag are considered.
4. No deformation occurs in the components of either body during collision.

2.1. Collision Forces Between the AUV and DOCK

In the ADAMS simulation environment, the collision force between the two components is computed directly using the built-in Impact function. The mathematical expression for the Impact function is defined as follows:

$$F_{\mathrm{n}} = K\delta^{n} + C\dot{\delta} \tag{1}$$

where F_n is the normal contact force, δ is the normal penetration depth, $\dot{\delta}$ is the normal relative velocity at the contact point, K is the contact stiffness, n is the nonlinear spring force exponent, and C is the damping coefficient. The contact stiffness, K, is calculated based on Hertz contact theory, expressed as follows:

$$K = \frac{4}{3\pi(h_1 + h_2)}\left(\frac{R_1 R_2}{R_1 + R_2}\right)^{1/2} \tag{2}$$

where R_1 and R_2 are the radii of curvature at the contact interface, and h_1 and h_2 are material parameters defined by $h_i = \frac{1-\mu_i^2}{\pi E_i}$, where μ_i is Poisson's ratio, and E_i is the elastic modulus for $\beth = 1, 2$.

The damping coefficient, C, is determined using the modified hysteresis damping coefficient proposed by Lankarani et al. [20], formulated as follows:

$$C = \frac{3K(1-e^2)}{4u_0}\delta^{n} \tag{3}$$

where e is the coefficient of restitution, and u_0 is the initial impact velocity.

Consequently, the final normal contact force can be expressed as follows [20].

$$F = K\delta^{n}\left[1 + \frac{3(1-e^2)}{4u_0}\dot{\delta}\right] \tag{4}$$

2.2. Hydrodynamic Drag on the Mooring Line

Axial forces generated by the water flow are neglected to simplify the dynamic model of the mooring line. Furthermore, the self-weight of the 10 m long, 1 cm diameter nylon line is approximately 0.9 kg, which is negligible relative to the total weight of the entire docking system. Based on the Morison equation, the force exerted on the mooring line is expressed as follows:

$$f = \frac{1}{2}\rho d C_d |v_c| v_c \tag{5}$$

where $= \rho$ is the fluid density, d is the diameter of the mooring line cross-section, C_d is the drag coefficient, and v_c is the horizontal flow velocity relative to the mooring line. By integrating Equation (5) over the length l, the total force acting on the mooring line is derived as follows [19].

$$F_d = \int_0^l f(v_c)dv \tag{6}$$

2.3. Hydrodynamic Drag on the DOCK and AUV

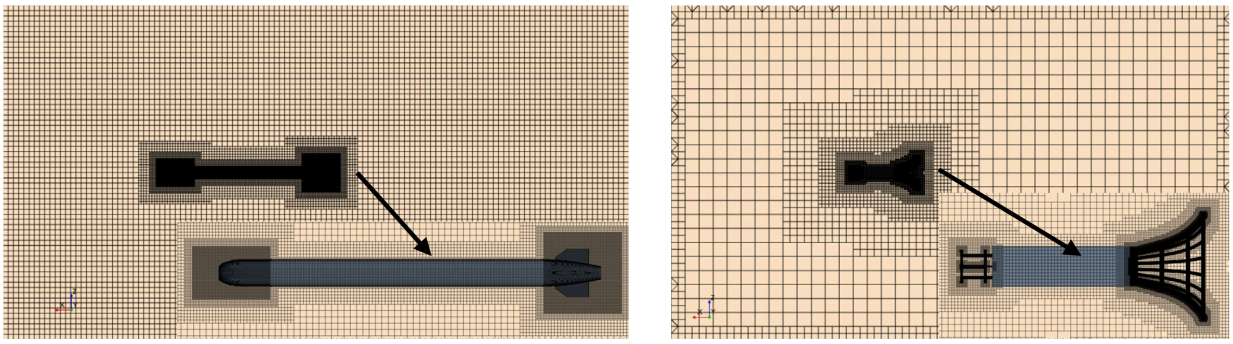
In ADAMS simulations involving fluid drag loads on AUVs or similar apparatuses, an added mass is typically applied as a mass force to simulate the inertial forces exerted via water flow on the AUV. However, because of the limited research on suspension docking systems and relative fixing of the DOCK to the seabed under various operating conditions, the added mass coefficient is omitted when configuring fluid drag loads for the DOCK.

This study adopted the standard submarine motion equations proposed by Gertler et al. [13], which have been validated extensively, as the formulation for calculating hydrodynamic forces.

$$\tau_h = [X_h Y_h Z_h K_h M_h N_h]^T \tag{7}$$

Detailed descriptions of the parameters can be found in reference [21]. Currently, the methods that exist for calculating hydrodynamic coefficients are the planar motion mechanism (PMM) method and the virtual planar motion mechanism (VPMM) or spatial constraint method. Both methods yield values with minimal error compared with experimentally measured values. The PMM method requires simulations across a sufficiently large number of diverse operating conditions, with the final precision improved by averaging the results. However, this approach may not fully reflect the effects of the geometry and hydrodynamic layout of the device on the coefficients. Although the VPMM method does not fully account for the fluid viscosity, it enables the determination of all hydrodynamic coefficients of the device through a single simulation case. Gao Ting et al. [22] used a computer equipped with a dual-core processor and 48 GB RAM and found that the PMM method required at least 12 simulation cases with a computation time extending to 10 days. In contrast, the VPMM method required only one case, with a computation time of approximately 65 h. Considering that this study primarily focused on the collision impact process and the available hardware resource for the research group was a 12-core processor with 32 GB RAM, the VPMM method was adopted to determine the hydrodynamic coefficients for the AUV and DOCK.

Figure 3 presents the mesh layout for the AUV and DOCK hydrodynamic coefficient calculation in STAR-CCM+. Mesh independence was verified using 1.68 million cells for the AUV and 3.68 million cells for the DOCK. The time step is 0.025 s and the total simulation duration is 250 s [2].



(**a**) AUV (188 w). (**b**) DOKC (368 w).

Figure 3. Mesh configuration of the hydrodynamic calculation model.

The analysis of spatially constrained motion is based on the nonlinear equations of spatial motion; therefore, it constitutes a multivariate nonlinear regression problem. Taking the force in the x-direction as an example, the nonlinear problem in Equation (8) can be transformed into a linear problem through appropriate variable substitution. The corresponding transformation formula is presented in Equation (9) [22].

$$X_h = \frac{1}{2}\rho L^4(X'_{qq}q^2 + X'_{rr}r^2 + X'_{rp}rp) + \frac{1}{2}\rho L^3(X'_{\dot{u}}\dot{u} + X'_{vr}vr + X'_{wq}wq) + \frac{1}{2}\rho L^2(X'_{uu}u^2 + X'_{vv}v^2 + X'_{ww}w^2) \quad (8)$$

$$x_1 = q^2, x_2 = r^2, x_3 = rp, x_4 = \dot{u}, x_5 = vr, x_6 = wq, x_7 = u^2, x_8 = v^2, x_9 = w^2 \quad (9)$$

The transformed linear equation is given as Equation (10) and is subsequently solved by multiple linear regression based on the least-squares method [22]:

$$X = a_0 + a_1x_1 + a_2x_2 + a_3x_3 + a_4x_4 + a_5x_5 + a_6x_6 + a_7x_7 + a_8x_8 + a_9x_9 \quad (10)$$

In this study, a linear-regression model for the motion equations was established using simulation data obtained between 20 and 200 s. The simulation results from 201 to 250 s were then used to validate the established linear-regression model. The resulting correlation coefficients were all close to unity, indicating that the identified hydrodynamic coefficients provide an accurate representation of the system dynamics. To eliminate excessive hydrodynamic coefficients, the least significant terms were progressively removed until the cutoff correlation coefficient fell below 0.95.

Using the aforementioned simplification procedures, the hydrodynamic coefficients for the AUV and the DOCK were reduced to the final expressions presented in Equations (11) and (12) [22].

$$\tau_{h1} = \begin{bmatrix} \frac{1}{2}\rho L^3 X'_{\dot{u}}\dot{u} + \frac{1}{2}\rho L^2 X'_{uu}u^2 \\ \frac{1}{2}\rho L^4(Y'_{\dot{r}}\dot{r} + Y'_{\dot{p}}\dot{p}) + \frac{1}{2}\rho L^3(Y'_{\dot{v}}\dot{v} + Y'_{ur}ur + Y'_{p}up) + \frac{1}{2}\rho L^2(Y'_{v}uv + Y'_{v|v|}v\left|\sqrt{v^2+w^2}\right|) \\ \frac{1}{2}\rho L^4 Z'_{\dot{q}}\dot{q} + \frac{1}{2}\rho L^3(Z'_{\dot{w}}\dot{w} + Z'_{q}uq) + \frac{1}{2}\rho L^2(Z'_{v}uv + Z'_{w}uw + Z'_{w|w|}w\left|\sqrt{v^2+w^2}\right|) \\ \frac{1}{2}\rho L^5(K'_{\dot{p}}\dot{p} + K'_{\dot{r}}\dot{r} + K'_{p|p|}p|p|) + \frac{1}{2}\rho L^4(K'_{p}up + K'_{r}ur + K'_{\dot{v}}\dot{v} + K'_{wp}wp + K'_{wr}wr) \\ \frac{1}{2}\rho L^5(M'_{\dot{q}}\dot{q} + M'_{rr}r^2 + M'_{rp}rp) + \frac{1}{2}\rho L^4(M'_{\dot{w}}\dot{w} + M'_{q}uq + M'_{w|q|}\left|\sqrt{v^2+w^2}\right|q) + \frac{1}{2}\rho L^3 M'_{w}uw \\ \frac{1}{2}\rho L^5(N'_{\dot{r}}\dot{r} + N'_{r|r|}r|r|) + \frac{1}{2}\rho L^4(N'_{\dot{v}}\dot{v} + N'_{r}ur + N'_{v|r|}\left|\sqrt{v^2+w^2}\right|r) \end{bmatrix} \quad (11)$$

$$\tau_{h2} = \begin{bmatrix} \frac{1}{2}\rho L^3 X'_{\dot{u}}\dot{u} + \frac{1}{2}\rho L^2 X'_{uu}u^2 \\ \frac{1}{2}\rho L^4(Y'_{\dot{r}}\dot{r} + Y'_{\dot{p}}\dot{p} + Y'_{qr}qr) + \frac{1}{2}\rho L^3(Y'_{\dot{v}}\dot{v} + Y'_{ur}ur) + \frac{1}{2}\rho L^2(Y'_{v}uv + Y'_{v|v|}v\left|\sqrt{v^2+w^2}\right|) \\ \frac{1}{2}\rho L^4 Z'_{\dot{q}}\dot{q} + \frac{1}{2}\rho L^3(Z'_{\dot{w}}\dot{w} + Z'_{q}uq + Z'_{w|q|}\frac{w}{|w|}\left|\sqrt{v^2+w^2}\right||q|) + \frac{1}{2}\rho L^2(Z'_{w}uw + Z'_{w|w|}w\left|\sqrt{v^2+w^2}\right|) \\ \frac{1}{2}\rho L^5(K'_{\dot{p}}\dot{p} + K'_{\dot{r}}\dot{r}) + \frac{1}{2}\rho L^4(K'_{ur}ur + K'_{\dot{v}}\dot{v} + K'_{wr}wr) + \frac{1}{2}\rho L^3(K'_{v}uv + K'_{v|v|}v\left|\sqrt{v^2+w^2}\right|) \\ \frac{1}{2}\rho L^5(M'_{\dot{q}}\dot{q} + M'_{q|q|}q|q|) + \frac{1}{2}\rho L^4(M'_{\dot{w}}\dot{w} + M'_{q}uq + M'_{w|q|}\left|\sqrt{v^2+w^2}\right|q) + \frac{1}{2}\rho L^3(M'_{w}uw + M'_{w|w|}w\left|\sqrt{v^2+w^2}\right|) \\ \frac{1}{2}\rho L^5(N'_{\dot{r}}\dot{r} + N'_{\dot{p}}\dot{p} + N'_{r|r|}r|r|) + \frac{1}{2}\rho L^4(N'_{\dot{v}}\dot{v} + N'_{r}ur) + \frac{1}{2}\rho L^3 N'_{v}uv \end{bmatrix} \quad (12)$$

In Equations (11) and (12), the symbols $X'(\cdot), Y'(\cdot), Z'(\cdot)$ represent the dimensionless hydrodynamic coefficients, and $K'(\cdot), M'(\cdot), N'(\cdot)$ represent the dimensionless hydrodynamic moment coefficients. Detailed definitions of these parameters are provided in "Submarine Maneuverability" [21]. The characteristic length, L, is 8.265 m for the AUV and 4.850 m for the DOCK.

2.4. Angular Momentum

The momentum theorem [23] was used to analyze the motion states of the AUV and DOCK. The derivative form of the angular momentum of an object is given by Equation (13):

$$\frac{d}{dt}L_0 = \sum_{i=1}^{n} M_0\left(F_i^{(e)}\right) = \sum_{i=1}^{n} r_i \times F_i^{(e)} \quad (13)$$

where L_0 is the angular momentum of the particle system of the object relative to a fixed point, and $\sum_{i=1}^{n} r_i \times F_i^{(e)}$ is the sum of the moments of external forces acting on the particle system relative to the fixed point. Equation (13) can be rewritten as follows:

$$dL_0 = \sum_{i=1}^{n} r_i \times F_i^{(e)} dt = \sum_{i=1}^{n} r_i \times dI_i^{(e)} \tag{14}$$

Upon integration, Equation (15) is derived.

$$\int_{L_{o2}}^{L_{o1}} dL_o = \sum_{i=1}^{n} \int_0^t r_i \times dI_i^{(e)} \tag{15}$$

Because this value is constant, it follows that Equation (16) is valid.

$$L_{o2} - L_{o1} = \sum_{i=1}^{n} r_i \times \int_0^t dI_i^{(e)} \tag{16}$$

Thus, the angular momentum during the collision between objects is formulated as follows:

$$L_{o2} - L_{o1} = \sum_{i=1}^{n} r_i \times I_i^{(e)} = \sum_{i=1}^{n} M_o\left(I_i^{(e)}\right) \tag{17}$$

where L_{01} and L_{02} are the angular momenta of the particle system of the object relative to the fixed point before and after the collision, respectively, $I_i^{()}$ is the collision impulse, and $r_i \times I_i^{()}$ represents the moment of the impulse.

3. Simulation Model of the Suspension Docking System

In contrast to docking systems in which the DOCK is fixed to the seabed, the simulation environment of the underwater suspension docking established using ADAMS necessitates the configuration of hydrodynamic drag loads for the AUV while simultaneously accounting for the effects of fluids on the DOCK. Consequently, there are two primary distinctions between the simulation environment settings for the suspension docking system and those for a static docking system. The first is the hydrodynamic drag configuration for the AUV and DOCK. The second is the modeling of the mooring line using a "discrete segment + flexible connection" approach, including the configuration for the transverse hydrodynamic drag of the mooring line.

3.1. Configuration of Hydrodynamic Drag Coefficients for Loads

A body-fixed coordinate system is first established for the DOCK (Figure 4) to configure the six-degree-of-freedom hydrodynamic drag forces acting on the DOCK. Subsequently, each hydrodynamic coefficient derived using the VPMM method is formulated as a mathematical function. These functions are then implemented in ADAMS using built-in functions, such as Acceleration X (ACCX) and Velocity X (VX), to construct explicit expressions for each degree of freedom. For example, the expression for the force along the X-axis is expressed by Xu_dt*ACCX (zhonglidian, 0, 0, ground.DD) + Xuu*VX (zhonglidian, 0, 0, ground.DD)**2. Detailed explanations regarding the application of functions, such as ACCX and VX, are provided in [24]. The procedure for configuring the hydrodynamic drag on the AUV is the same as that for the DOCK. Under steady-state conditions at a constant speed of 0.25 kn, the required main propeller thrust is approximately 6 N. The simplified hydrodynamic coefficients for the AUV and DOCK are presented in Tables 1 and 2, respectively.

Table 1. Hydrodynamic drag coefficient of AUV.

$X'_{\dot{u}} = -0.00022$	$X'_{uu} = -0.00101$	$Y'_{\dot{r}}\dot{r} = 0.00242$	$Y'_{\dot{p}}\dot{p} = 0.00016$	$Y'_{\dot{v}}\dot{v} = -0.00793$	$Y'_{ur} = 0.01724$	$Y'_{p} = 0.00019$
$Y'_{v} = -0.02409$	$Y'_{v\|v\|} = -0.00286$	$Z'_{\dot{q}} = -0.00295$	$Z'_{\dot{w}} = -0.00867$	$Z'_{q} = -0.02627$	$Z'_{v} = 0.00011$	$Z'_{w} = -0.00111$
$Z'_{w\|w\|} = -0.03365$	$K'_{\dot{p}} = -0.00005$	$K'_{\dot{r}} = -0.00004$	$K'_{p\|p\|} = -0.00245$	$K'_{p} = -0.00504$	$K'_{r} = -0.03042$	$K'_{\dot{v}} = 0.00157$
$K'_{wp} = -0.00158$	$K'_{wr} = 0.00048$	$M'_{\dot{q}} = -0.00171$	$M'_{rr} = 0.00147$	$M'_{rp} = 0.00477$	$M'_{\dot{w}} = -0.00299$	$M'_{q} = -0.01385$
$M'_{w\|q\|} = 0.08591$	$M'_{w} = -0.01988$	$N'_{\dot{r}} = -0.00134$	$N'_{r\|r\|} = -0.00661$	$N'_{\dot{v}} = 0.00247$	$N'_{r} = -0.00917$	$N'_{v\|r\|} = -0.00392$

Table 2. Hydrodynamic drag coefficient of DOCK.

$X'_{\dot{u}} = -0.00827$	$X'_{uu} = -0.04725$	$Y'_{\dot{r}}\dot{r} = -0.01184$	$Y'_{\dot{p}}\dot{p} = 0.00231$	$Y'_{qr} = -0.04084$	$Y'_{\dot{v}}\dot{v} = -0.03250$	$Y'_{ur} = -0.00046$
$Y'_{v} = 0.01213$	$Y'_{v\|v\|} = -0.16476$	$Z'_{\dot{q}} = 0.00991$	$Z'_{\dot{w}} = -0.03561$	$Z'_{q} = 0.02728$	$Z'_{w\|q\|} = 0.00576$	$Z'_{w} = -0.06846$
$Z'_{w\|w\|} = -0.10558$	$K'_{\dot{p}} = -0.00020$	$K'_{\dot{r}} = 0.00039$	$K'_{ur} = 0.00113$	$K'_{\dot{v}} = 0.00132$	$K'_{wr} = -0.00293$	$K'_{v} = 0.00272$
$K'_{v\|v\|} = 0.00461$	$M'_{\dot{q}} = -0.00502$	$M'_{q\|q\|} = 0.00242$	$M'_{\dot{w}} = 0.00992$	$M'_{q} = -0.01822$	$M'_{w\|q\|} = -0.54146$	$M'_{w} = -0.00161$
$M'_{w\|w\|} = 0.03050$	$N'_{\dot{r}} = -0.02525$	$N'_{p} = -0.00525$	$N'_{r\|r\|} = 0.00047$	$N'_{\dot{v}} = -0.00400$	$N'_{r} = -0.01125$	$N'_{v} = -0.03660$

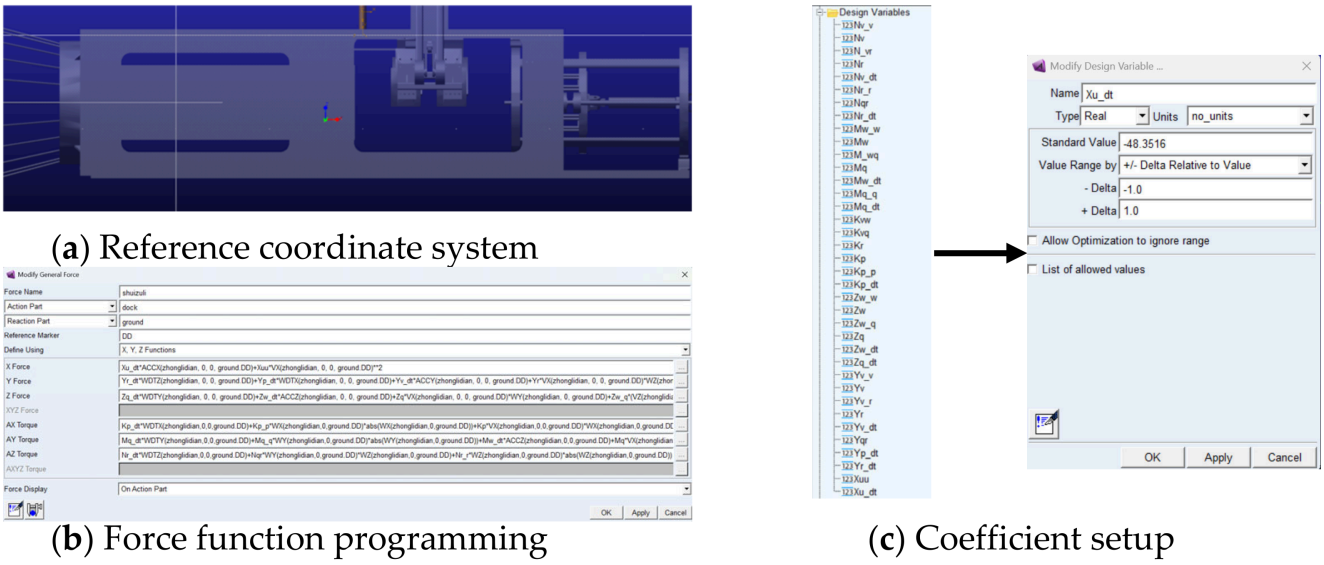


Figure 4. Hydrodynamic drag coefficient settings interface.

3.2. Discretization of the Mooring Line and Load Settings

In this study, the mooring line of the suspension docking system was modeled using a "discrete segment + flexible connection" approach. Specifically, a nylon rope with a total length of 15 m and a diameter of 1 cm was discretized into 150 equal-length rigid cylindrical elements, each measuring 100 mm in length, and sequentially labeled as gss_1 through gss_150. Material properties, interelement bushing connections, and hydrodynamic drag forces were assigned to each segment via customized scripting.

A total of 149 flexible connections were established between adjacent mooring line segments using bushing force elements (Figure 5). The axial tensile stiffness and damping characteristics of the nylon rope must be explicitly defined. The axial tensile stiffness of 19,634.95 N/mm was calculated as the product of the elastic modulus of the nylon rope (E = 3.0 GPa) and the cross-sectional area of the selected mooring line. The axial damping coefficient is set to 5% of the axial tensile stiffness (981.75 N·s/mm), consistent with the empirical damping ratio for nylon flexible cables recommended in the OrcaFlex software manual [25] and previous marine dynamic studies. This proportional damping

configuration accurately reproduces the internal frictional energy dissipation of nylon fiber while suppressing unrealistic numerical oscillation during dynamic simulations.

Furthermore, in accordance with the OrcaFlex software manual [25] and Wang et al. [26], the shear, bending, and torsional stiffness values were set to a near-zero baseline range of 5–10 N/mm. In this study, the minimum value of 5 N/mm within this interval was adopted. This value closely approximates the ideal fully flexible behavior of a nylon rope while avoiding additional bending and shear resistance associated with larger stiffness values. Meanwhile, the use of a small nonzero stiffness prevents numerical singularities and improves the stability of the ADAMS bushing force calculations. This ensures that the rope can freely undergo swinging, bending, and twisting motions, thereby accurately replicating the behavior of a flexible underwater mooring line. Based on Morison's equation, ADAMS command scripts were employed to iteratively apply customized lateral hydrodynamic drag forces at the center of mass of each discrete segment, enabling efficient implementation of fluid resistance across the entire mooring line. The resulting model constitutes a discretized, flexible tether suitable for simulating underwater suspension docking operations. Critical parameters used in defining the bushing connections and hydrodynamic drag for the mooring line model are summarized in Table 3.

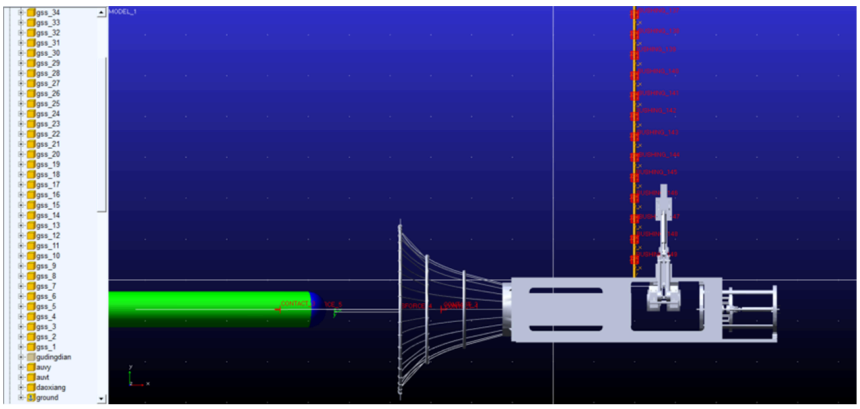


Figure 5. Mooring line establishment diagram.

Table 3. Critical parameters of the mooring line.

Parameter	Value
Axial Tensile Stiffness (N/mm)	19,634.95
Axial Damping (N·s/mm)	981.75
Shear/Bending/Torsional Stiffness (N/mm)	5.00
Fluid Density ρ (kg/mm^3)	0.999 $\times 10^{-6}$
Drag Coefficient C_d	1.2

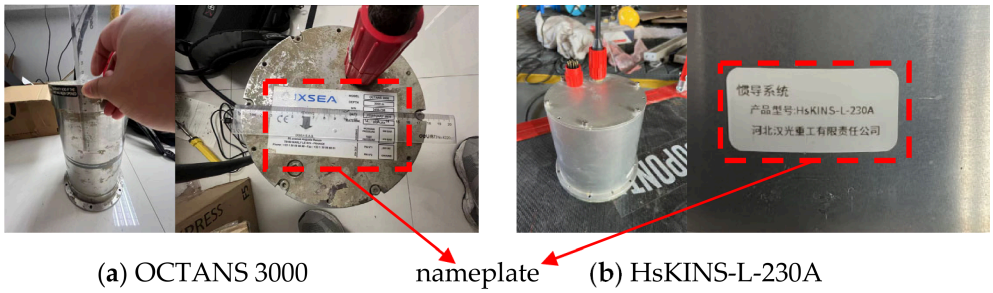
4. Water Tank Experiments

Suspension docking collision experiments were conducted at the water tank facility of the Shenyang Institute of Automation, Chinese Academy of Sciences, to validate the proposed simulation model. The dimensions of the water tank were 100 m (length) × 50 m (width) × 15 m (depth).

4.1. Equipment

The physical prototypes of the DOCK and AUV used in the water tank experiments are shown in Figure 1a,b, respectively. Following structural modifications and ballast adjustments, the final masses of the AUV and DOCK were 1084 and 898 kg, respectively. The DOCK was equipped with two redundant sensors (an OCTANS 3000 sensor (Exail, Marly-

le-Roi, France) and an HsKINS-L-230A sensor (Hebei Hanguang Heavy Industry, Handan, China)) to mitigate the risk of single-point sensor failure (Figure 6). Data acquisition was performed at a sampling frequency of 15 Hz.



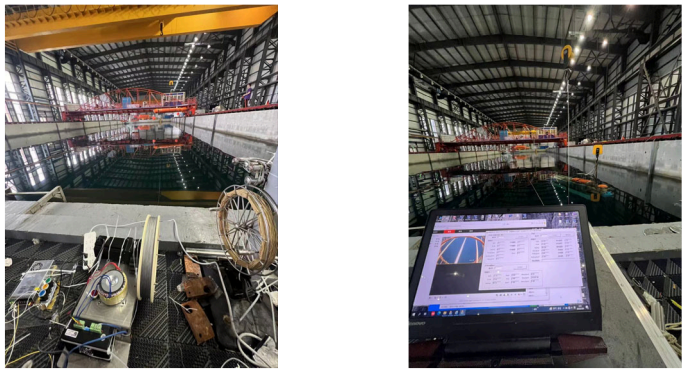
(**a**) OCTANS 3000 nameplate (**b**) HsKINS-L-230A

Figure 6. Sensor model.

4.2. Method

The overall layout of the water tank experiment is shown in Figure 6. After ballasting, the DOCK exhibited a negative buoyancy of approximately 2000 N. The DOCK was deployed into the water using a dual-hook mechanism. Upon stabilization, its static attitude satisfied the following criteria: a roll angle smaller than $\pm 1.5°$ and a pitch angle smaller than $\pm 2°$. At the commencement of each trial, the AUV was positioned approximately 30 m from the DOCK. A winch driven by a stepper motor towed the AUV at a constant velocity toward the DOCK to induce collision; the forward speed of the AUV was controlled by adjusting the rotational speed of the stepper motor (Figure 7a). In addition, the initial yaw angle was modulated by altering the initial heading orientation of the DOCK (Figure 7b). The flowchart of the docking test is shown in Figure 8.

Based on methodologies established in previous studies, a single-variable experimental design was adopted to identify key factors influencing the collision response during the suspension docking process. The analyzed variables included the collision velocity, eccentricity, and initial offset angle, alongside intrinsic system properties, such as the moment of inertia and mass ratio. Consequently, five distinct types of experimental scenarios were investigated. To minimize random experimental errors, at least three replicate experiments were conducted under each operating condition. The average of the three experimental measurements was used for comparison with the numerical simulation results, and the mean relative error (MRE) between the experimental averages and the simulation results was calculated to quantify the accuracy of the proposed model. Following comprehensive data processing and analysis, over 200 valid collision events were identified and retained for further examination.



(**a**) Traction winch drawing. (**b**) Underwater deployment mode.

Figure 7. The overall layout of the water tank experiment diagram.

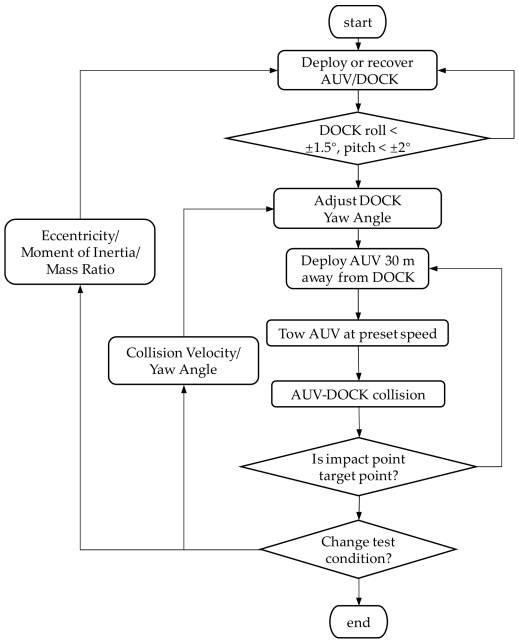


Figure 8. The flowchart of the docking test.

5. Data Comparison and Analysis

Unlike static docking stations, which are fixed to the seabed, a suspended DOCK is susceptible to excessive separation after collision if the AUV approaches at a very high velocity. This separation potentially leads to docking failure. The yaw angular velocity ω_h of the DOCK immediately following the initial collision event during suspension docking was selected as the primary validation parameter to verify the validity of the simulation model.

5.1. Effect of Collision Velocity (v_o) on Collision Response

Based on the prior experience of the research group in shallow-water-docking operations, the optimal approach velocity for the AUV should not be lower than 0.5 kn or higher than 2.0 kn [27]. Accordingly, the AUV approach velocities were set to 0.5, 0.6, 0.7, 0.8, 0.9, 1.0, 1.1, and 1.2 kn, considering the capability of the experimental setup. The horizontal eccentricity (d_h), vertical eccentricity (d_v), and yaw angle (θ_o) were fixed to 1000 mm, 0 mm, and 0°, respectively.

The simulation results and water-tank experimental results are presented in Table 4. The simulation results were consistent with the experimental results; the average MRE was 4.06% (Table 4). Under conditions where all other parameters remained constant, a decrease in collision velocity corresponded to a proportional decrease in the post-collision yaw angular velocity (ω_h) of the DOCK.

Table 4. ω_h under different collision velocities.

Collision Velocity (kn)	Experimental Values (°/s)	Experimental Average (°/s)	Simulation Values (°/s)	MRE (%)
0.5	2.82/2.59/2.68	2.70	2.43	10.00
0.6	3.29/3.07/3.02	3.13	3.21	2.56
0.7	3.79/3.81/3.87	3.82	3.70	3.14
0.8	4.25/4.05/4.36	4.22	4.43	4.98
0.9	4.71/4.58/4.65	4.65	4.75	2.15
1.0	5.10/5.01/5.21	5.11	5.28	3.33
1.1	5.67/5.55/5.59	5.60	5.76	2.86
1.2	6.11/6.44/6.41	6.32	6.10	3.48

5.2. Effect of Eccentricity (d_o) on Collision Response

Eccentricity (d_o) comprises two components (Figure 2b): horizontal eccentricity (d_h) and vertical eccentricity (d_v). The following subsections discuss these components separately. The collision velocity (v_o) was maintained at 1 kn, and the yaw angle (θ_o) was fixed to 0°, adhering to the principle of single controlling variables.

5.2.1. Effect of Horizontal Eccentricity (d_h) on Collision Response

Because of constraints within the experimental environment, the vertical eccentricity (d_v) was fixed to 0 mm. For the water tank experiments, the selected horizontal eccentricities (d_h) were 1000, 900, 800, and 700 mm. Subsequent values of 600, 500, 400, 300, 200, and 100 mm were evaluated exclusively using the simulation model.

A comparative summary of the simulation and experimental results is presented in Table 5. Based on the four sets of data presented above, the average MRE was 10.53%. The data indicate that a decrease in only the horizontal eccentricity results in a decreased angular velocity of the DOCK, thereby facilitating suspension docking. However, achieving such smaller eccentricities presupposes a higher degree of control precision for the AUV.

Table 5. ω_h under different horizontal eccentricities.

Horizontal Eccentricity (mm)	Experimental Values (°/s)	Experimental Average (°/s)	Simulation Values (°/s)	MRE (%)
1000	5.10/5.19/4.96	5.08	5.28	3.94
900	4.51/4.43/4.48	4.47	4.77	6.71
800	4.08/4.12/3.97	4.06	4.48	10.34
700	3.45/3.52/3.15	3.37	3.98	18.10
600	2.97/3.18/2.71	2.95	3.35	13.56
500	-	-	3.02	-
400	-	-	2.64	-
300	-	-	2.15	-
200	-	-	2.01	-
100	-	-	1.75	-

5.2.2. Effect of Vertical Eccentricity (d_v) on Collision Response

Analogous to the evaluation of horizontal eccentricity d_h, the horizontal component (d_h) was fixed to 0 mm. The vertical eccentricity (d_v) ranged from 1000 to 100 mm in intervals of 100 mm. Similarly, for the vertical eccentricity range of 600 to 100 mm, only simulation data were available. Given that a horizontal eccentricity of 0 mm yields a post-collision yaw angular velocity close to 0°/s for the DOCK, the pitch angular velocity (ω_p) was selected as the validation parameter.

The average MRE was 7.31% (Table 6). As the vertical eccentricity decreased, the post-collision pitch angular velocity (ω_p) decreased correspondingly. Although collisions in the vertical direction induce larger sudden variations in pitch angular velocity ω_p compared with ω_h, the inherent high metacentric height of the DOCK facilitates rapid recovery of its pitch angle.

Taking the static docking trial data from a lake test reported in [8] as a representative case (Figure 9), the depth-keeping accuracy of the AUV, while cruising at a low speed of 0.25 kn, remained within 0.1 m. Given that the vertical control precision of the AUV exceeds its horizontal counterpart, this paper prioritizes the analysis of the impact of horizontal offset on the success criteria for suspension docking and the associated collision response characteristics.

Docking simulations were performed for AUV velocities of 0.5 and 2 kn at a horizontal offset of 860 mm, with the initial collision defined as t = 0 (Figure 10). Contact between the AUV bow and the endpoint of the DOCK docking pipe confirms successful berthing (Figure 10d). In contrast, Figure 10h depicts a gradual separation between the AUV and DOCK; in the absence of external intervention, this scenario is classified as docking failure.

Table 6. ω_p under different vertical eccentricities.

Vertical Eccentricity (mm)	Experimental Values (°/s)	Experimental Average (°/s)	Simulation Values (°/s)	MRE (%)
1000	14.51/14.35/14.38	14.41	15.11	4.86
900	12.62/12.66/12.53	12.60	13.71	8.81
800	11.35/11.51/11.48	11.45	12.51	9.26
700	10.23/10.19/10.06	10.16	11.00	8.27
600	9.04/9.01/9.35	9.13	9.62	5.37
500	-	-	7.80	-
400	-	-	7.41	-
300	-	-	6.16	-
200	-	-	4.77	-
100	-	-	3.63	-

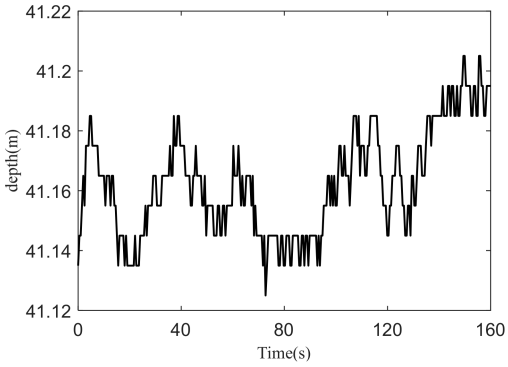
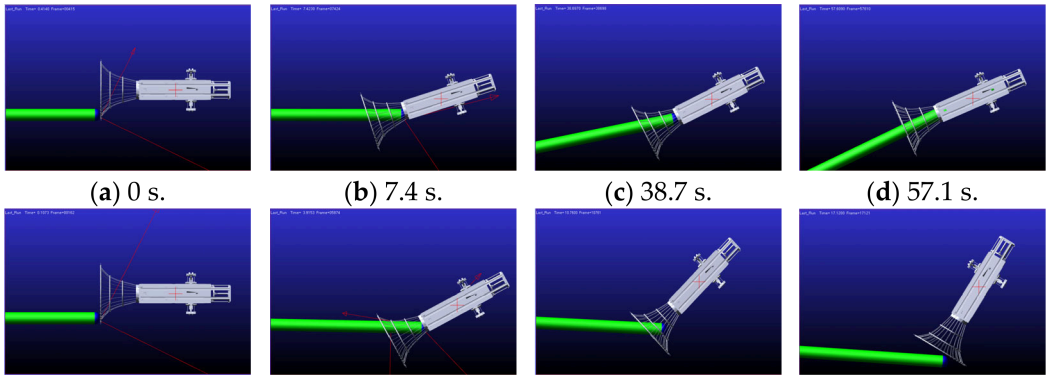


Figure 9. Depth curve of AUV low-speed constant-depth navigation in the lake test.



(**a**) 0 s. (**b**) 7.4 s. (**c**) 38.7 s. (**d**) 57.1 s.

(**e**) 0 s. (**f**) 3.9 s. (**g**) 10.7 s. (**h**) 17.1 s.

Figure 10. Simulation diagram of AUV docking.

5.3. Effect of Yaw Angle (θ_o) on Collision Response

All other parameters were kept constant (collision velocity [v_o]: 1 kn; horizontal eccentricity [d_h]: 1000 mm; vertical eccentricity [d_v]: 0 mm) to evaluate the effect of yaw angle (θ_o) on collision response. Considering practical docking scenarios where excessive yaw angles typically lead to the abortion of the current attempt in favor of a redocking maneuver, the selected yaw angles (θ_o) were 0°, 5°, 10°, 15°, 30°, 45°, 60°, and 75°.

A comparative summary of the simulation and experimental results is provided in Table 7. The average MRE between the experimental and simulated values was 6.14% (Table 7). As the yaw angle increased, the yaw angular velocity (ω_h) initially increased and subsequently decreased, reaching its peak when the yaw angle θ_o approached 45°. Therefore, docking should be aborted if the pre-docking yaw angle of the AUV reaches or exceeds 45° in the absence of external forces, and preparations for a subsequent mission should be initiated.

Table 7. ω_h under different yaw angles.

Yaw Angle (°)	Experimental Values (°/s)	Experimental Average (°/s)	Simulation Values (°/s)	MRE (%)
0	5.10/5.06/5.12	5.09	5.28	3.73
5	6.81/6.87/6.63	6.77	6.55	3.25
10	7.99/8.61/8.65	8.42	7.87	6.53
15	8.94/8.12/8.36	8.47	9.52	12.40
30	10.88/10.97/10.94	10.93	10.31	5.67
45	11.32/11.01/11.20	11.18	11.50	2.86
60	10.85/10.69/10.81	10.78	10.04	6.86
75	9.92/10.17/10.47	10.19	9.39	7.85

5.4. Effect of Moment of Inertia (I_d) on Collision Response

Equation (1) shows that the moment of inertia directly influences the variation in the rotational angular velocity of the DOCK. Five water tank experiments were conducted in accordance with experimental constraints to ensure the invariance of other initial conditions, such as mass ratio and negative buoyancy. In these experiments, four 100 kg weights were sequentially relocated from the center of gravity of the DOCK to the endpoints of the DOCK frame. Following each relocation, the increment in the moment of inertia (ΔI_d) of the DOCK was approximately 4×10^8 kg·mm^2. The collision conditions were defined as follows: collision velocity (v_o): 1 kn; yaw angle (θ_o): 0°, horizontal eccentricity (d_h): 1000 mm; and vertical eccentricity (d_v): 0 mm.

The average MRE between the simulation and experimental results was 6.48% (Table 8). As the moment of inertia of the DOCK increased, the motion tendency of the DOCK under identical conditions was significantly attenuated (Table 8). Specifically, an increased moment of inertia yielded a decreased variation in the yaw angular velocity (ω_h) of the DOCK, which is beneficial for suspension docking. Therefore, provided that structural stability is maintained, appropriately increasing the moment of inertia of the DOCK is recommended.

Table 8. ω_h under different moments of inertia.

Moment of Inertia (kg·mm^2)	Experimental Values (°/s)	Experimental Average (°/s)	Simulation Values (°/s)	MRE (%)
0	4.42/4.31/4.38	4.37	4.58	4.81
4×10^8	3.78/3.66/4.01	3.82	3.95	3.40
8×10^8	3.21/3.23/3.17	3.20	3.50	9.38
1.2×10^9	2.97/2.84/2.89	2.90	3.12	7.59
1.6×10^9	2.58/2.66/2.69	2.64	2.83	7.20

5.5. Effect of Mass Ratio on Collision Response

The effect of mass on collision response was examined by progressively removing the four 100 kg weights previously added to the center of gravity of the DOCK for the moment of inertia examination, while monitoring the changes in the yaw angular velocity (ω_h) of the DOCK. The docking conditions were consistent with those described in Section 5.4.

The average MRE was 4.58% (Table 9). Table 9 presents a comparative summary of the simulation and experimental results of the mass ratio. As the DOCK mass increased gradually, the variation in ω_h was insignificant (Table 9). In contrast, the translational velocity (v) of the DOCK after collision exhibited more pronounced changes.

Table 9. ω_h under different mass ratios.

Mass Ratio (AUV:DOCK)	Experimental Values (°/s)	Experimental Average (°/s)	Simulation Values (°/s)	MRE (%)
1.204	5.10/5.00/5.03	5.04	5.28	4.76
1.084	4.89/4.96/4.77	4.87	5.09	4.52
0.985	4.71/4.68/4.43	4.61	4.90	6.29
0.903	4.55/4.39/4.61	4.52	4.72	4.42
0.834	4.42/4.48/4.46	4.45	4.58	2.92

The average MRE was 12.64% (Table 10). Table 10 presents a comparative summary of the simulation and experimental results for the effect of mass ratio on translational velocity. As the mass ratio decreased, the variation in the post-collision translational velocity of the DOCK decreased significantly. This indicates that during suspension docking, a smaller mass ratio between the two entities is more favorable for achieving a stable docking operation.

Table 10. Translational velocity (v) under different mass ratios.

Mass Ratio (AUV:DOCK)	Experimental Values (m/s)	Experimental Average (m/s)	Simulation Values (m/s)	MRE (%)
1.204	0.45/0.41/0.40	0.42	0.51	21.43
1.084	0.40/0.36/0.37	0.38	0.44	15.79
0.985	0.34/0.33/0.35	0.34	0.38	11.76
0.903	0.31/0.32/0.34	0.32	0.33	3.13
0.834	0.28/0.27/0.25	0.27	0.30	11.11

6. Conclusions

A comparative analysis between empirical data obtained from water tank experiments and computational results derived from ADAMS simulations has validated the efficiency and reliability of the proposed simulation model. In this study, the verified model was used to analyze collision responses under diverse operating conditions.

This study revealed that, during suspension docking between an underactuated, axisymmetric 534 mm AUV and a single-point-moored DOCK in still water, excessive collision velocity, yaw angle, and eccentricity generated significant eccentric loading moments on the DOCK. These forces trigger overall rotational instability, severely compromising docking attitude stability and ultimately leading to docking failure. Consequently, the effects of various operating conditions on docking collisions and the effects of critical parameters within the docking system, specifically the mass ratio, negative buoyancy, and mooring line length, were evaluated. The following conclusions can be drawn.

1. Under conditions at which the initial yaw angle is 0° and no vertical eccentricity exists, the maximum permissible horizontal offset for successful docking at an AUV velocity of 0.5 kn is 860 mm; exceeding this threshold leads to docking failure. The corresponding maximum horizontal eccentricity at 2 kn decreases to 610 mm, considering practical engineering constraints in which docking velocities typically do not exceed 2 kn.
2. In practical docking operations, maintaining an initial yaw angle of exactly 0° is challenging. Assuming an initial AUV velocity of 0.5 kn and zero vertical eccentricity, the maximum allowable horizontal eccentricities corresponding to initial yaw angles of 0°, 5°, 10°, and 15° are 860, 790, 630, and 180 mm, respectively, under the premise of successful docking. These findings indicate that as the initial yaw angle increases from 10° to 15°, the requirements for the horizontal navigation accuracy of the AUV become significantly more stringent.

3. With determined docking conditions, the intrinsic structural properties of the docking system also critically influence the results. An insufficient DOCK mass results in excessive post-collision translational and angular velocities, hastening docking failure. The simulation results indicate that at a collision velocity of 0.5 kn, yaw angle of 5°, horizontal eccentricity of 790 mm, and zero vertical eccentricity of the AUV, reducing the DOCK mass to approximately 500 kg (while maintaining a constant AUV mass) renders docking unachievable. Therefore, it is recommended that the AUV:DOCK mass ratio remains lower than two. When masses are fixed, maximizing the moment of inertia of the DOCK is advisable. With constant masses for both the AUV and DOCK, progressively increasing the moment of inertia of the DOCK enhances the capacity of the system to maintain its original state (Table 8), thereby effectively reducing the time consumption of the docking process. The recorded docking durations decreased sequentially from 53.1, 50.5, 47.8, and 45.2 s to 42.3 s.
4. An excessive mooring line length also contributes to docking failure. Furthermore, the docking duration increases proportionally with mooring line length. Using the initial conditions from Conclusion (3) as a baseline, increasing the mooring line length from 15 m to 25 m extended the docking duration from 53.1 s to 75.8 s. Docking failure occurs when the mooring line exceeds 28.6 m.
5. During the docking process, increased negative buoyancy of the DOCK correlates with enhanced attitude stability. If the negative buoyancy of the DOCK decreases below 300 N, the docking mission fails under the operating conditions specified in Conclusion (3).
6. When docking with a fixed base station, increasing the main thrust of the AUV can accelerate berthing. However, in a suspension docking system where the DOCK is not rigidly connected to the seabed, an excessive main thrust leads to docking failure. The simulation results demonstrate that when the main thrust exceeds 18 N, the docking system fails under the conditions outlined in Conclusion (3).

This study has several limitations that can be addressed in future work. First, all simulations and experiments were performed under ideal quiescent-water conditions. Future research will incorporate diverse current and wave conditions to explore the dynamic docking performance and environmental adaptability of the suspended docking system under realistic ocean conditions. Second, limited by the size of the experimental tank, the AUV could not navigate autonomously during tests, and external propulsion was adopted for collision experiments. Therefore, the full self-propelled docking process could not be completely reproduced in the current study. Third, this work only evaluated the dynamic docking performance without considering engineering economic constraints. Increasing the moment of inertia and negative buoyancy improves docking stability but raises manufacturing and deployment costs; future studies will introduce economic boundary conditions to balance docking performance and practical engineering costs. Fourth, the investigation was confined to fixed-size underactuated axisymmetric AUVs. Subsequent research will extend the analysis to AUVs of various sizes and configurations to validate the universality and robustness of the proposed docking system.

Author Contributions: Conceptualization, H.T. and R.Z.; methodology, H.T. and R.Z.; software, H.T.; validation, H.T., Z.L. and G.Z.; formal analysis, H.T.; investigation, H.T. and R.Z.; resources, R.Z.; data curation, H.T.; writing—original draft preparation, H.T.; writing—review and editing, R.Z.; visualization, H.T. and Z.L.; supervision, R.Z.; project administration, Z.L.; funding acquisition, R.Z. All authors have read and agreed to the published version of the manuscript.

Funding: This research was funded by the Strategic Priority Research Program of the Chinese Academy of Sciences (XDA0310000).

Data Availability Statement: Data are contained within the article.

Conflicts of Interest: The authors declare no conflicts of interest.

Abbreviations

The following abbreviations are used in this manuscript:

AUV	autonomous underwater vehicle
AUVs	autonomous underwater vehicles
DOCK	guiding hood docking device
PMM	planar motion mechanism
VPMM	virtual planar motion mechanism
ACCX	Acceleration X
VX	Velocity X
MRE	mean relative error

References

1. Feng, X.; Li, S. *Autonomous Underwater Vehicle*; Science Press: Beijing, China, 2019.
2. Zheng, R.; Tan, H.; Lv, Z.; Xu, H.; Yu, Z. Dynamic characteristics of deep-sea single-point mooring levitation docking system. *Ocean Eng.* **2024**, *301*, 117536.
3. Meng, L. *Research on Dynamic Characteristics of Autonomous Recovery of UUV by USV*; Shenyang Institute of Automation, Chinese Academy of Sciences: Shenyang, China, 2019.
4. Yazdani, A.M.; Sammut, K.; Yakimenko, O.; Lammas, A. A survey of underwater docking guidance systems. *Robot. Auton. Syst.* **2020**, *124*, 103382. [CrossRef]
5. Chen, R.Y.; Zhang, Y.L. Analysis on Docking Collision Between AUV and Towed Recovery Dock. *Chin. J. Ship Res.* **2026**, *21*, 226–239.
6. Guo, J.Q.; Meng, L.S.; Feng, M.M.; Liu, J.; Peng, Z.; Feng, W.; Cui, J.-H. Dynamic Characteristic Analysis of Underwater Suspended Docking Station for Resident UUVs. *J. Mar. Sci. Eng.* **2024**, *12*, 1493. [CrossRef]
7. Wu, L.H.; Li, Y.P.; Su, S.J.; Yan, P.; Qin, Y. Hydrodynamic Analysis of AUV Underwater Docking with a Cone-shaped Dock under Ocean Currents. *Ocean Eng.* **2014**, *85*, 110–126. [CrossRef]
8. Gao, Y.; Li, X.H.; Mei, J.W.; Lu, D.; Tang, Y. Hydrodynamic Numerical Analysis of AUV Underwater Docking with Conical Docking Bay. *J. Mar. Sci. Eng.* **2025**, *13*, 1645. [CrossRef]
9. Lin, M.W.; Lin, R.; Yang, C.J.; Li, D.; Zhang, Z.; Zhao, Y.; Ding, W. Docking to An Underwater Suspended Charging Station: Systematic Design and Experimental Tests. *Ocean Eng.* **2022**, *249*, 110766. [CrossRef]
10. Guo, J.Q.; Tan, H.; Liu, J.; Feng, W.; Peng, Z.; Liu, Y.; Cui, J.-H. Numerical Simulation and Analysis of UUV Docking with a Seabed Moored Floating Dock. *Ocean Eng.* **2024**, *313*, 119528. [CrossRef]
11. Guo, J.; Zheng, R.; Lv, H. AUV Underwater Docking Collision Analysis and Guidance Structure Optimization Based on ADAMS Simulation. *Acta Armamentarii* **2019**, *40*, 1058–1067.
12. Wang, X. Modeling Analysis and Control of Collision in Underwater Robot Docking Operations. Master's Thesis, Jiangsu University of Science and Technology, Jiangsu, China, 2020.
13. Shi, J.; Li, D.; Yang, C.; Cai, Y. Impact Analysis during Docking Process of Autonomous Underwater Vehicle. *J. Zhejiang Univ. (Eng. Sci.)* **2015**, *49*, 497–504.
14. Li, K. Research on Key Technologies of AUV Underwater Docking and Docking Collision Issues. Master's Thesis, Harbin Engineering University, Harbin, China, 2017.
15. Yuan, M. Research on Petal-like Mechanical Gripper for Underwater Recovery of AUVs. Master's Thesis, Tianjin University, Tianjin, China, 2023.
16. Li, C. Modeling of Docking Collision for Underwater Unmanned Vehicle Recovery and Design of Manipulator. Master's Thesis, Lanzhou University of Technology, Lanzhou, China, 2025.
17. Pan, W. Research on Collision and Control of Underwater Robot Mobile Docking. Master's Thesis, Jiangsu University of Science and Technology, Jiangsu, China, 2022.
18. Wang, C. Design and Key Technology Research of Unmanned Underwater Vehicle Recovery Platform. Master's Thesis, Jiangsu University of Science and Technology, Jiangsu, China, 2025.
19. Guo, J. Research on Key Technologies of AUV Underwater Docking Device. Master's Thesis, Northeastern University, Shenyang, China, 2019.

20. Zhang, Y.; Tang, Y.; Yao, Z. Collision Analysis and Cover-Type Docking Platform Optimization Design in the Underwater Docking Process of Portable AUVs. *J. Mar. Sci. Technol.* **2017**, *36*, 27–31.
21. Shi, S. *Submarine Maneuverability*; National Defense Industry Press: Beijing, China, 2003.
22. Gao, T.; Pang, Y.; Wang, Y.; Chen, Q. Calculation Method of Hydrodynamic Coefficients for Underwater Vehicles. *J. Harbin Eng. Univ.* **2019**, *40*, 174–180.
23. Chen, Z. Research on the Buffering Device for AUV Underwater Docking Based on Small Hole Throttling. Master's Thesis, Harbin Engineering University, Harbin, China, 2024.
24. Li, Z.; Li, B. *ADAMS: A Comprehensive Introduction with Practical Examples*, 3rd ed.; Tsinghua University Press: Beijing, China, 2021.
25. Orcina Ltd. *OrcaFlex User Manual*; Orcina Ltd.: Cumbria, UK, 2025.
26. Wang, B.; Chen, Y.; Yu, F. Dynamic Simulation Analysis and Verification of the Attitude of Deep-sea Mooring Buoys. *Mar. Sci.* **2021**, *45*, 1–8.
27. Anderlini, E.; Parker, G.G.; Thomas, G. Docking control of an autonomous underwater vehicle using reinforcement learning. *Appl. Sci.* **2019**, *9*, 3456. [CrossRef]

Disclaimer/Publisher's Note: The statements, opinions and data contained in all publications are solely those of the individual author(s) and contributor(s) and not of MDPI and/or the editor(s). MDPI and/or the editor(s) disclaim responsibility for any injury to people or property resulting from any ideas, methods, instructions or products referred to in the content.